Journal of Alloys and Compounds 527 (2012) 106–111

Contents lists available at SciVerse ScienceDirect

Journal of Alloys and Compounds

journal homepage: www.elsevier.com/locate/jallcom

Fabrication, characterization and photocatalytic properties of Ag nanoparticles modified TiO_2 NTs

Qingyao Wang, Xiuchun Yang*, Dan Liu, Jianfu Zhao

School of Materials Science and Engineering, Tongji University, Shanghai 201804, People's Republic of China

ARTICLE INFO

Article history:
Received 10 November 2011
Received in revised form 26 February 2012
Accepted 28 February 2012
Available online xxx

Keywords:
TiO_2 NTs
Ag nanoparticles
Successive ionic layer adsorption and reaction
Photocatalytic degradation

ABSTRACT

Ordered anatase TiO_2 nanotubes (TiO_2 NTs) on Ti substrate were synthesized by electrochemical anodization and subsequently vapor-thermal treatment. Ag nanoparticles were decorated on TiO_2 NTs by successive ionic layer adsorption and reaction (SILAR) technique. Raman spectroscopy, X-ray absorption near edge spectroscopy (XANES), X-ray diffraction (XRD), UV–vis diffuse reflectance spectroscopy, scanning electron microscopy (SEM) and transmission electron microscopy (TEM) were used for the characterization of surface morphology, phase composition, and microstructure of the original TiO_2 NTs, the vapor-thermally treated TiO_2 NTs and the Ag nanoparticles decorated TiO_2 NTs. The results indicate that vapor-thermal treatment favors to the transformation of amorphous TiO_2 into anatase phase. Increasing the SILAR cycle times favors to increase the loaded amounts of Ag nanoparticles in TiO_2 NTs. Ag nanoparticles are uniformly distributed in the TiO_2 NTs, and the SILAR process does not damage the ordered tubular structure. A possible formation mechanism of Ag/TiO_2 NTs has also been proposed. The photocatalytic results showed that the Ag nanoparticle modified TiO_2 NTs largely enhanced the photocatalytic degradation of methyl orange under ultraviolet light irradiation.

1. Introduction

In recent years, TiO_2 NTs are the most extensively studied material due to their unique electronic and optical properties, which can be applied in photocatalyst, biosensor, dye-sensitized solar cells and other applications [1–5]. Many methods, such as anodization [6–8], template technique [9], hydrothermal process [10–12], and soft chemical process [13] have been used to prepare TiO_2 NTs. The development of highly ordered TiO_2 NTs by a simple and green electrochemical anodization has shown many advantages in providing high surface area and efficient unidirectional charge transport routes, thus generating extensive technological interest [14,15].

TiO_2 NTs have been widely studied as a model system for a range of photocatalytic processes [16–18]. However, the rapid recombination of photoinduced electrons and holes greatly lowers the effective applications of TiO_2 NTs. Recently, noble metals decorated TiO_2 NTs have received increasing attention due to their promotion of the separation of photogenerated electron–hole pairs and thus enhancement of the photocatalytic activity of TiO_2 NTs [1,19–22]. Silver (Ag) particles are often applied to act as electron reservoirs to suppress the electron–hole pairs recombination, thus more holes are available for the oxidation reactions, which cause a lot of attention in the modification of TiO_2 NTs [23]. In recent years, Xie et al. adopted a pulse current deposition technique to construct highly dispersed Ag nanoparticles on TiO_2 NTs [24]. Liang et al. successfully fabricated Ag nanoparticles in self-organized TiO_2 NTs by a simple wet reduction method [25]. Paramasivam et al. investigated Ag nanoparticles loaded onto self-organized TiO_2 NTs under continuous UV irradiation [26]. The above three methods are the most familiar strategies to synthesize the Ag nanoparticles loaded TiO_2 NTs. The successive ionic layer adsorption and reaction (SILAR) technique is a more convenient and novel method, which is used to construct the uniform distribution of metal sulfide nanoparticles in the TiO_2 NTs. However, by the best of our knowledge, no literature reported the fabrication of noble metal nanoparticle decorated TiO_2 NTs by the SILAR route.

In the paper, the SILAR method was used to homogeneously decorate the TiO_2 NTs with Ag nanoparticles of about 9.2 nm. The effects of different deposition cycles on the essential structures and properties of the Ag/TiO_2 NTs were systematically investigated. The photocatalytic activity of the synthesized Ag/TiO_2 NTs was also tested by using the liquid-phase photocatalytic degradation of methylene orange (MO) as a model reaction.

2. Experimental details

2.1. Preparation of self-organized TiO_2 NTs

Self-organized TiO_2 NTs were prepared by a two-step anodization of titanium foil (0.25 mm thickness, 99.8% purity), following the typical procedure [27]. The

* Corresponding author. Tel.: +86 21 69580446.
E-mail address: yangxc@tongji.edu.cn (X. Yang).

0925-8388/$ – see front matter © 2012 Elsevier B.V. All rights reserved.
doi:10.1016/j.jallcom.2012.02.180

first-step anodization was performed under 60 V for 1 h in ethylene glycol solution containing 0.5 wt.% NH_4F and 3 vol.% H_2O. After the first step, the as-formed TiO_2 NTs were peeled off by intense ultrasonication in deionized water to expose the Ti substrate. The second-step anodization was carried out in the same conditions as mentioned above for 4 h. The TiO_2 NTs were then vapor-thermally treated at different temperatures for 6 h [28].

2.2. Surface modification of TiO_2 NTs

The vapor-thermally treated TiO_2 NTs at 180 °C were immersed in 0.3 M mercaptoacetic acid solution for 30 min. Afterwards, the TiO_2 NTs containing mercaptoacetic acid were dried at 60 °C for 10 h.

2.3. Synthesis of Ag-sensitized TiO_2 NTs

The mercaptoacetic acid modified TiO_2 NTs were sequentially sensitized with Ag by using SILAR technique. First, TiO_2 NTs were dipped into 0.2 M $AgNO_3$ solution for 5 min, rinsed with deionized water, then dipped for another 5 min into 0.15 M $NaBH_4$ solution and again rinsed with deionized water. This whole procedure is referred to as one full SILAR cycle. For comparison, this SILAR processes for 5, 10 and 15 times were denoted as Ag(5)/TiO_2 NTs, Ag(10)/TiO_2 NTs and Ag(15)/TiO_2 NTs, respectively.

2.4. Characterization

The phase compositions of samples were determined by a Rigaku D/Max 2400 X-ray diffractometer (XRD) equipped with graphite monochromatized Cu Kα radiation. Renishaw System 1000 Raman microscope was used to collect Raman data of samples using 514.5 nm laser light from a He:Ne laser. Ti K-edge XANES spectra were collected in transmission mode with a Si (1 1 1) double-crystal monochromator at the 4WIB beam line of Shanghai Synchrotron Radiation Facility. The morphology and element composition of samples were directly observed by a Quanta 200 FEG scanning electron microscope (SEM) equipped with energy dispersive spectroscope (EDS). Microstructure was characterized by a FEI Tecnai F30 transmission electron microscope (TEM) operated at an accelerating voltage of 300 kV. UV–vis diffuse reflectance spectra (DRS) were recorded on a UV-4100 UV-vis spectrophotometer with an integrating sphere attachment. $BaSO_4$ was used as a reflectance standard in the wavelength range of 200–800 nm.

2.5. Photocatalytic activity test

The photocatalytic activity of the prepared samples was evaluated by photocatalytic decomposition of 30 mL MO (5×10^{-5} M) aqueous solution under 250 W UV irradiation (λ = 254 nm). Before photodegradation, adsorption equilibrium of the dye on the sample with area of 1.54 cm^2 was established by ultrasonication for 1 min and then mechanical stirring for 30 min in the dark environment. The change in MO concentration was monitored by determining the UV–visible adsorption of 3.0 mL sample taken from the solution every 10 min at 464 nm. After measurement, the sample was put back to the reaction solution to conduct the photo-degradation experiments with the same procedure as mentioned above.

3. Results and discussion

The formation of anatase crystalline phase under vapor-thermal treatment was confirmed by Raman spectra (Fig. 1a) and XANES spectra (Fig. 1b). Sample NT-1 has a weak and broad Raman peak at 615 cm^{-1}, indicating that the vapor-thermally treated TiO_2 NTs at 100 °C is mainly composed of amorphous TiO_2. Samples NT-2 and NT-3 have three obvious Raman peaks at 399, 516 and 639 cm^{-1}, corresponding quite well to the typical Raman signals of anatase [3,29]. Raman peak intensity increases with increasing vapor-thermal temperature, indicating that anatase crystallization degree is improved. Ti K-edge XANES spectrum of the original TiO_2 NTs has a big pre-edge peak with a small shoulder, which reveals that the original TiO_2 NTs are amorphous. Three small pre-edge peaks marked as A_1, A_2 and A_3 appear after vapor-thermally treating the amorphous TiO_2 NTs at 180 °C. The three pre-edge peaks are consistent with that of the anatase reference, which originate from the forbidden transitions from the core 1 s level to unoccupied 3d states of a Ti (IV) [30]. The results indicate that the amorphous TiO_2 NTs can transform into anatase phase after vapor-thermal treatment, which is consistent with the previous result [28].

The typical XRD patterns of the vapor-thermally treated TiO_2 NTs and Ag-decorated TiO_2 NTs with different cycle times are shown in Fig. 2. Pattern (a) indicates that the original TiO_2 transformed into anatase after vapor-thermal treatment at 180 °C. The average size of the TiO_2 crystalline was calculated to be approximately 11 nm from the (1 0 1) peak by using the Scherrer equation. Patterns (b), (c) and (d) indicate that new diffraction peaks appear at 38.2°, 44.3°, 64.6°, 77.5° and 81.6°, corresponding to (1 1 1), (2 0 0), (2 2 0), (3 1 1) and (2 2 2) facets of Ag (JCPDS 04-0783), respectively. The peak intensity of Ag increases with the increase of cycle times due to an increasing amount of Ag nanoparticles. Additionally, further observation indicates that the big diffraction peak at 38.2° appears overlapping, which is from the three diffraction peaks of TiO_2 (0 0 4) = 37.8, Ag (1 1 1) = 38.1° and TiO_2 (1 1 2) = 38.6°.

The SEM image of the original TiO_2 NTs as shown in Fig. 3a indicates that the TiO_2 NTs are vertically oriented with a diameter of approximately 137 nm and a wall thickness of about 30 nm. A side-view of the original TiO_2 NTs as shown in Fig. 3b indicates that all walls are entirely smooth. Fig. 3c shows the bottom image of the original TiO_2 NTs with an ordered hexagonal structure. Fig. 3e–g gives SEM images of Ag(10)/TiO_2 NTs, indicating that Ag nanoparticles are uniformly distributed in the TiO_2 NTs, and the deposition process does not damage the ordered tubular structure. Specially, TiO_2 crystal grains are obvious on the bottom of the Ag loaded TiO_2 NTs because that vapor-thermal treatment can induce the nucleation and growth of TiO_2 in the amorphous barrier lay. The EDS spectra (Fig. 3d and h) indicate that the original TiO_2 NTs are composed of Ti and O elements, and the Ag decorated TiO_2 NTs are composed of elements Ti, O, S and 31 at.% Ag. The S element is from the linker mercaptoacetic acid.

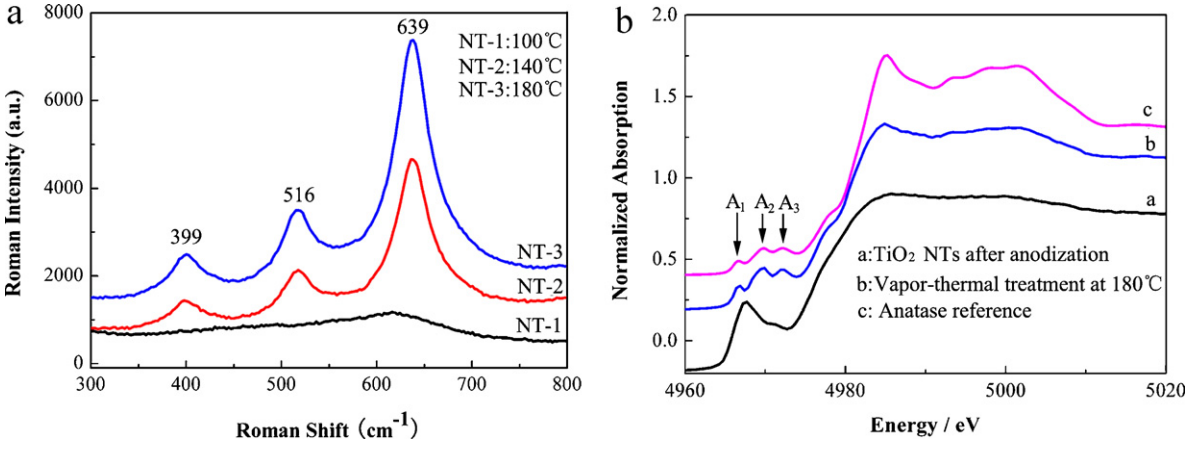

Fig. 1. Raman spectra (a) and Ti K edge XANES spectra (b) of the original TiO_2 NTs and the vapor-thermally treated TiO_2 NTs.

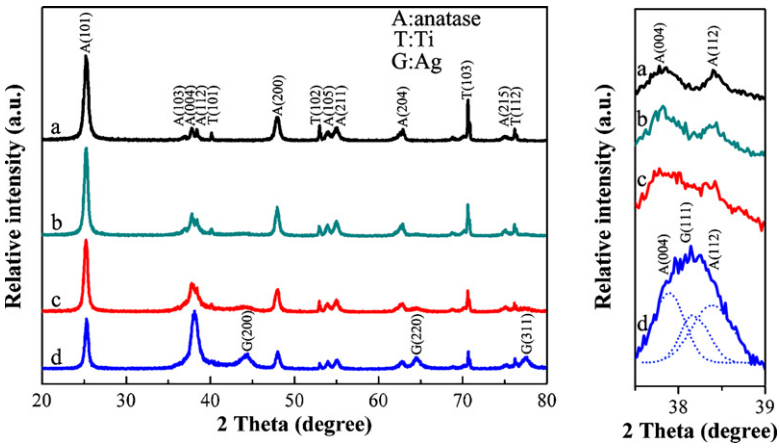

Fig. 2. XRD patterns of the vapor-thermally treated TiO_2 NTs (a), Ag(5)/TiO_2 NTs (b), Ag(10)/TiO_2 NTs (c), and Ag(15)/TiO_2 NTs (d). The right are the enlarged XRD patterns of the vapor-thermally treated TiO_2 NTs and Ag/TiO_2 NTs at $2\theta = 37.5–39^\circ$.

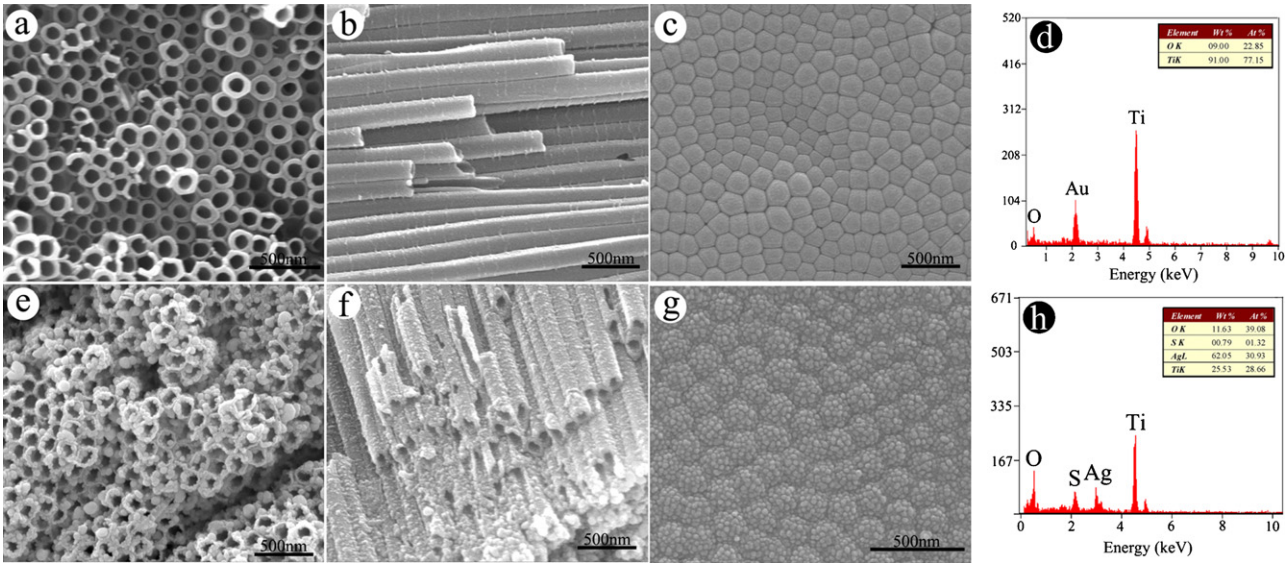

Fig. 3. SEM images and EDS spectra of the vapor-thermally treated TiO_2 NTs (a–d) and Ag(10)/TiO_2 NTs (e–h). (a, e): top views, (b, f): cross-section views, (c, g): bottom views, and (d, h): EDS spectra.

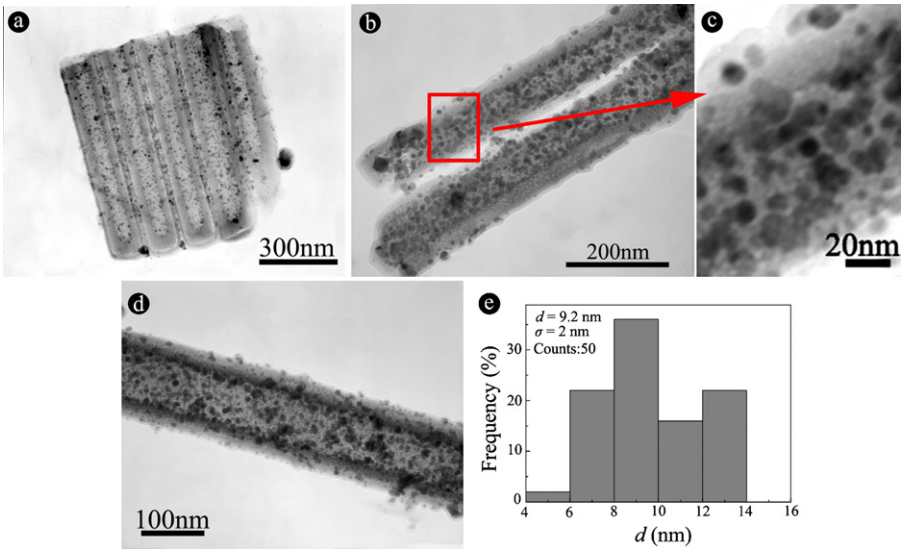

Fig. 4. TEM images of Ag(10)/TiO_2 NTs: the panorama (a), front-side (b) and middle region (d). HRTEM image of Ag(10)/TiO_2 NTs (c) and size distribution of Ag nanoparticles (e).

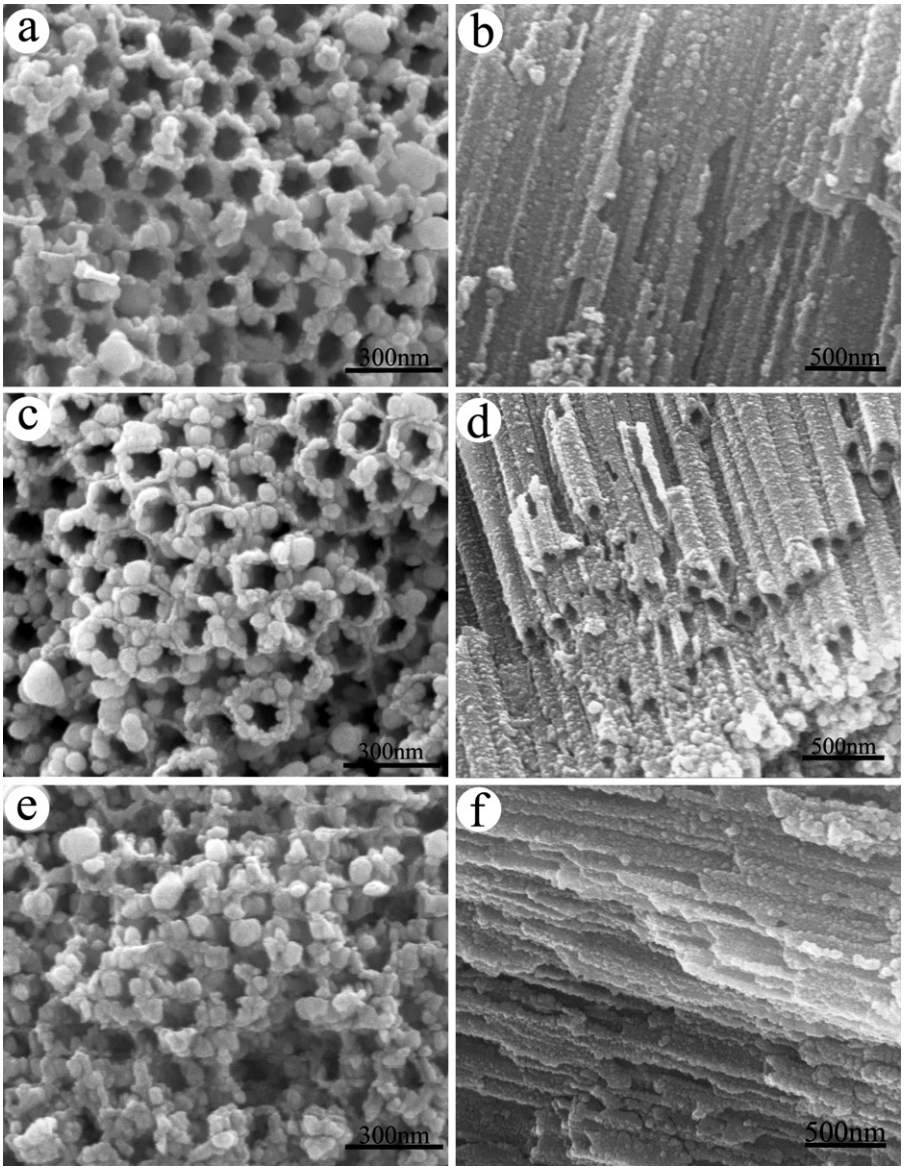

Fig. 5. SEM images of Ag(5)/TiO_2 NTs (a, b), Ag(10)/TiO_2 NTs (c, d), and Ag(15)/TiO_2 NTs (e, f). Left: top views; right: cross-section views.

Ag(10)/TiO_2 NTs were further investigated by TEM as shown in Fig. 4. It clearly displays that Ag nanoparticles with an average diameter of 9.2 nm uniformly distributed on the whole inner walls.

Fig. 5 gives SEM images of Ag decorated TiO_2 NTs after 5, 10 and 15 cycles, respectively. As shown in Fig. 5a and b, only a few Ag nanoparticles are deposited on the surface and inner walls of Ag(5)/TiO_2 NTs. However, after 10 cycles, the nanotube surface becomes extensively coated with relatively uniform Ag nanoparticles. Further increase deposition to 15 cycles, obvious agglomerations of Ag nanoparticles are observed on the top surface of TiO_2 NTs.

Our strategy to fabricate the Ag/TiO_2NTs can be schematically shown in Fig. 6. The vapor-thermally treated TiO_2 NTs were first treated with bi-functional mercaptoacetic acid linkers (HOOC–R–S). The –OH group on the surface of TiO_2 NT provides a strong affinity with the carboxylate group in the linker molecules. The thiol functional group in the linker molecules facilitates the binding with Ag from $AgNO_3$ solution. After Ag^+ ions were reduced by $NaBH_4$, Ag nanoparticles formed by nucleation and growth. The corresponding chemical reaction is as follows:

$$4Ag^+ + BH_4^- + 3H_2O \rightarrow 4Ag\downarrow + B(OH)_3 + 2H_2\uparrow + 3H^+$$

Fig. 7 gives the UV–vis absorption spectra of the vapor-thermally treated TiO_2 NTs and Ag nanoparticles sensitized TiO_2 NTs for different deposition cycles. Fig. 7a shows that the vapor-thermally treated TiO_2 NTs primarily absorb ultraviolet light below 387 nm due to its intrinsic band gap of 3.2 eV. Ag nanoparticle decorated TiO_2 NTs display a broad absorption peak centered at 470 nm, which originates from surface plasmon resonance (SPR) of Ag nanoparticles [31]. SPR intensity increases with increasing the SILAR cycle times due to the increase of the loaded amounts of Ag nanoparticles in TiO_2 NTs.

To evaluate the photocatalytic degradation capability of Ag/TiO_2 NTs, we examined the decomposition of MO in water under UV light irradiation (Fig. 8a). For comparison purposes, photodegradation

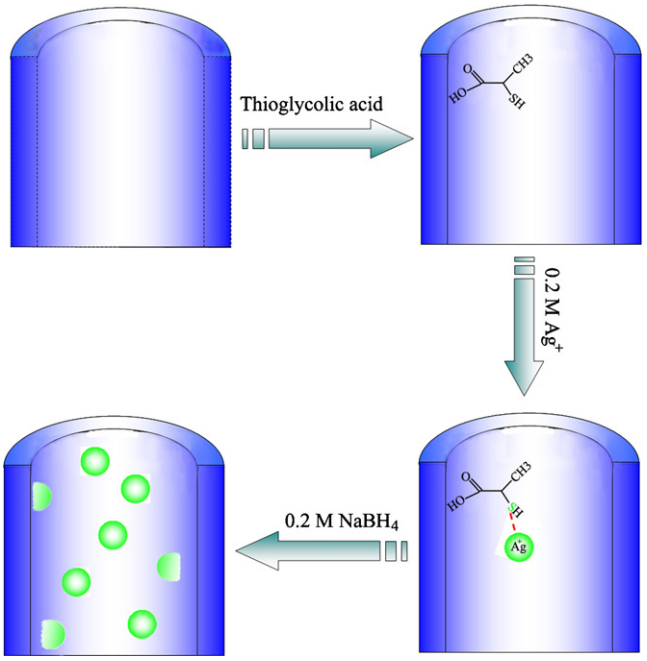

Fig. 6. Schematic diagram of Ag nanoparticle formation in TiO_2 NTs.

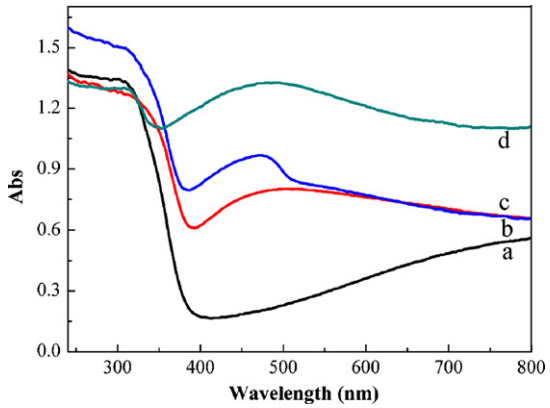

Fig. 7. UV–vis spectra of the vapor-thermally treated TiO_2 NTs (a), Ag(5)/TiO_2 NTs (b), Ag(10)/TiO_2 NTs (c), and Ag(15)/TiO_2 NTs (d).

of the dye without any photocatalyst was researched, and its final photodegradation rate was less than 13%. After 70 min of UV irradiation, 91% of MO was decomposed by Ag(10)/TiO_2 NTs, only 78%, 71% and 71% of MO was decomposed by Ag(5)/TiO_2 NTs, Ag(15)/TiO_2 NTs and the vapor-thermally treated TiO_2 NTs, respectively. It indicates that Ag(10)/TiO_2 NTs exhibit the highest photocatalytic capability in degrading MO dye under the UV irradiation. The principle of Ag/TiO_2 NTs photocatalytic decomposition of MO is illustrated in Fig. 8b. Because the Fermi level of Ag nanoparticles is lower than the conduction band of anatase TiO_2, photoexcited electrons can transfer from the conduction band of the TiO_2 towards Ag nanoparticles and accumulate there to form a Schottky barrier between the TiO_2 NTs and the Ag nanoparticles [1]. The photogenerated electrons accumulated on Ag nanoparticles surface have a good fluidity and could easily transfer to the absorbed oxygen on Ag surface forming O_2^- active groups, which favors the photocatalytic process. Holes accumulate in the valence band of the TiO_2, which are available for the oxidation reactions. This progress greatly reduces the possibility of electron–hole recombination, resulting in efficient separation and higher photocatalytic activity [32]. However, excessive Ag particles loaded TiO_2 NTs result in a lower efficiency, which could be attributed two reasons. One is that excess Ag deposits on the surface of TiO_2 NTs energetically capable of trapping photoelectrons decrease charge carrier space distance and thereby increase recombination [33]. The other is that the excess loading of Ag nanoparticles may cover active sites on the TiO_2 surface thereby reducing photodegradation efficiency [34]. This result testifies that Ag(10)/TiO_2 NTs achieve the highest efficiency of photocatalysis, which is attributed to plasmon–exciton coupling between anchored Ag nanoparticles co-catalysts and the host TiO_2.

4. Conclusions

In summary, we have successfully decorated TiO_2 NTs with Ag nanoparticles by a strategy combining the electrochemical anodic process and the ionic layer adsorption and reaction route. The vapor-thermal treatment favors to the transformation of amorphous TiO_2 into anatase phase. Increasing the SILAR cycle times favors to increase the loaded amounts of Ag nanoparticles in TiO_2 NTs. Ag nanoparticles with an average diameter of 9.2 nm are uniformly distributed in the TiO_2 NTs with an average diameter of about 137 nm, and the SILAR process does not damage the ordered tubular structure. The Ag nanoparticle modified TiO_2 NTs largely enhanced the photocatalytic degradation of methyl orange under ultraviolet light irradiation.

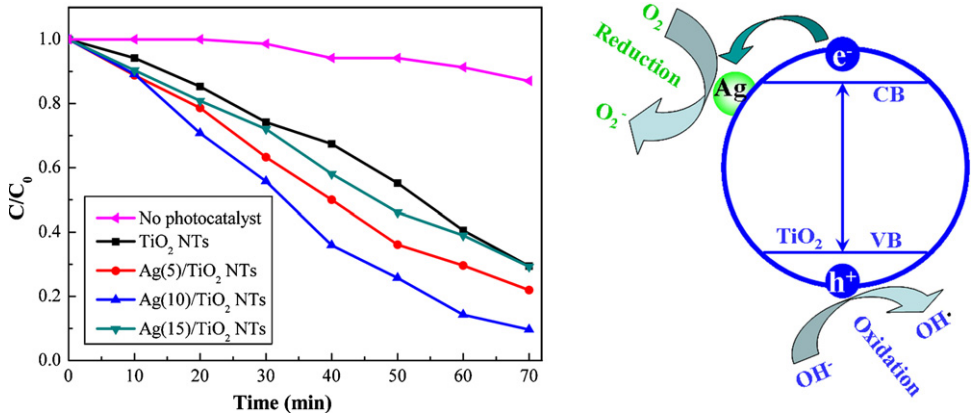

Fig. 8. (a) Photocatalytic degradation curves of MO on Ag/TiO_2NTs and (b) schematic diagram of the interface charge-carrier transfer of photocatalysis for Ag/TiO_2NTs.

Acknowledgments

This work was financially supported by Key Item for Basic Research of Shanghai (No. 05JC14058), the National Natural Science Foundation of China (No. 50672069) and the Nanotechnology Special foundation of Shanghai (No. 11 nm0500700).

References

[1] X.L. He, Y.Y. Cai, H.M. Zhang, C.H. Liang, J. Mater. Chem. 21 (2011) 475.
[2] J.C. Koh, Z.A. Ahmad, A.A. Mohamad, J. Alloys Compd. 509 (2011) 8707.
[3] J. Wang, Z.Q. Lin, Chem. Mater. 22 (2010) 579.
[4] P. Zhong, W.X. Que, J. Zhang, Q.Y. Jia, W.J. Wang, Y.L. Liao, X. Hu, J. Alloys Compd. 509 (2011) 7808.
[5] X.W. Zeng, Y.X. Gan, E. Clark, L.S. Su, J. Alloys Compd. 509 (2011) L221.
[6] J.R. Deneault, X.Y. Xiao, T.S. Kang, J.S. Wang, C.M. Wai, G.J. Brown, M.F. Durstock, ChemPhysChem 13 (2012) 256.
[7] H. Yang, C.X. Pan, J. Alloys Compd. 501 (2010) L8.
[8] Z. Lockmana, S. Sreekantana, S. Ismail, L.S. Mende, J.L. Driscoll, J. Alloys Compd. 503 (2010) 359.
[9] J.J. Qiu, W.D. Yu, X.D. Gao, X.M. Li, Nanotechnology 17 (2006) 4695.
[10] H. Jiang, J.Q. Hu, F. Gu, C.Z. Li, J. Alloys Compd. 478 (2009) 550.
[11] M. Myahkostupov, M. Zamkov, F.N. Castellano, Energy Environ. Sci. 4 (2011) 998.
[12] H. Jiang, T. Zhao, C.Z. Li, J. Ma, J. Mater. Chem. 21 (2011) 3818.
[13] M.D. Wei, Y. Konishi, H.S. Zhou, H. Sugihara, H. Arakawa, Solid State Commun. 133 (2005) 493.
[14] J.M. Macak, S.P. Albu, P. Schmuki, Phys. Status Solidi RRL 1 (2007) 181.
[15] J. Wang, Z.Q. Lin, Chem. Mater. 20 (2008) 1257.
[16] A.G. Kontos, A. Katsanaki, T. Maggos, V. Likodimos, A. Ghicov, D. Kimc, J. Kunze, C. Vasilakos, P. Schmuki, P. Falaras, Chem. Phys. Lett. 490 (2010) 58.
[17] Y.J. Chen, G.H. Tian, K. Pan, C.G. Tian, J. Zhou, W. Zhou, Z.Y. Ren, H.G. Fu, Dalton Trans. 41 (2012) 1020.
[18] Z.Y. Liu, X.T. Zhang, S. Nishimoto, T. Murakami, A. Fujishima, Environ. Sci. Technol. 42 (2008) 8547.
[19] R.E. Rettew, N.K. Allam, F.M. Alamgir, ACS Appl. Mater. Interfaces 3 (2011) 147.
[20] Y.Y. Song, Z.D. Gao, P. Schmuki, Electrochem. Commun. 13 (2011) 290.
[21] J.M. Macak, F.S. Stein, P. Schmuki, Electrochem. Commun. 9 (2007) 1783.
[22] X.H. Li, G.Y. Chen, L.B. Yang, Z. Jin, J.H. Liu, Adv. Funct. Mater. 20 (2010) 2815.
[23] Y.C Liang, C.C. Wang, C.C. Kei, Y.C. Hsueh, W.H. Cho, T.P. Perng, J. Phys. Chem. C 115 (2011) 9498.
[24] K.P. Xie, L. Sun, C.L. Wang, Y.K. Lai, M.Y. Wang, H.B. Chen, C.J. Lin, Electrochim. Acta 55 (2010) 7211.
[25] Y.Q. Liang, Z.D. Cui, S.L. Zhu, Y. Liu, X.J. Yang, J. Catal. 278 (2011) 276.
[26] I. Paramasivam, J.M. Macak, A. Ghicov, P. Schmuki, Chem. Phys. Lett. 445 (2007) 233.
[27] Q.Y. Wang, X.C. Yang, X.L. Wang, M. Huang, J.W. Hou, Electrochim. Acta 62 (2012) 158.
[28] J.G. Yu, G.P. Dai, B. Cheng, J. Phys. Chem. C 114 (2010) 19378.
[29] L. Sun, J. Li, C.L. Wang, S.F. Li, H.B. Chen, C.J. Lin, Sol. Energy Mater. Sol. Cells 93 (2009) 1875.
[30] T. Kubo, A. Nakahira, J. Phys. Chem. C 112 (2008) 1658.
[31] Y.K. Lai, H.F. Zhuang, K.P. Xie, D.G. Gong, Y.X. Tang, L. Sun, C.J. Lin, Z. Chen, New J. Chem. 34 (2010) 1335.
[32] G.S. Mital, T. Manoj, Chin. Sci. Bull. 56 (2011) 1639.
[33] M. Sadeghi, W. Liu, T.G. Zhong, P. Stavropoulos, B. Levy, J. Phys. Chem. 100 (1996) 19466.
[34] S. Sakthivel, M.V. Shankar, M. Palanichamy, B. Arabindoo, D.W. Bahnemann, V. Murugesan, Water Res. 38 (2004) 3001.